Numerical Study of Non-equilibrium Phase Transitions in Active Brownian Particles

Paswa Nath

A Thesis Submitted to

Indian Institute of Technology Hyderabad

In Partial Fulfillment of the Requirements for

The Degree of Master of Science

भारतीय प्रौद्योगिकी संस्थान हैदराबाद

Indian Institute of Technology Hyderabad

Department of Physics

April 2015

Declaration

I declare that this written submission represents my ideas in my own words, and where ideas or words of others have been included, I have adequately cited and referenced the original sources. I also declare that I have adhered to all principles of academic honesty and integrity and have not misrepresented or fabricated or falsified any idea/data/fact/source in my submission. I understand that any violation of the above will be a cause for disciplinary action by the Institute and can also evoke penal action from the sources that have thus not been properly cited, or from whom proper permission has not been taken when needed.

_____

(Signature)

Paswa Nath

_____

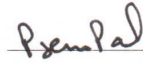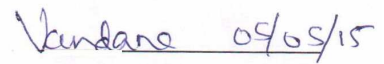(Paswa Nath)

PH13M1009

_____

(Roll No.)

Approval Sheet

This Thesis entitled Numerical Study of Non-equilibrium Phase Transitions in Active Brownian Particles by Paswa Nath is approved for the degree of Master of Science from IIT Hyderabad
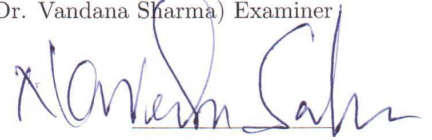
(Dr. Debasish Chaudhuri) Advisor
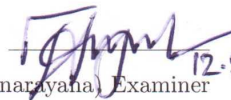
(Dr. Prem Pal) Examiner

09/05/15

(Dr. Vandana Sharma) Examiner

(Dr. Narendra Sahu) Examiner

(Dr. Jyoti Ranjan Mohanty) Examiner

12.5.15

(Dr. J. Suryanarayana) Examiner

(Dr. S Hundi) Examiner

(Dr. Sai Santosh Kumar Raavi) Examiner

Acknowledgements

First of all, I do acknowledge my supervisor, Dr. Debasish Chaudhuri, for guiding me and encouraging me throughout in this project and for giving me the courage and confidence to deal with difficult problems through theory and computation. The experience that I gained in this one year of work is perhaps the most precious thing that I'll take away.

And of course I can't leave any one of my 14 classmates unacknowledged for their own way of encouragement and support for me, especially at the time of *"segmentation faults"* either in real or in virtual world! I should specially mention Pradeep Valicherla here, with whom I had some very illuminating discussions.

Last but not the least, I do acknowledge my parents who never asked about my progress, they only asked whether I'm enjoying my work not. I would not have taken computational physics that seriously if I never came across a book named *On Beauty* by Umberto Eco which showed various patterns and fractals, bridging visual arts to science, which my father used to explain me one by one.

Abstract

In this report we present our work on athermal phase separation of active Brownian particles through Molecular Dynamics simulations using a model by Merchetti et. al. We identified and characterized the solid-fluid phase transitions taking place in the active system. We spent a significant amount of time in parallelizing the molecular dynamics simulations which allowed us to work with larger system spending less time for computation. We investigated various structural properties of the overall system and of the two co-existing phases through clustering analysis. And finally we worked with active systems under confinement and showed that they behave differently than that of their passive counterparts.

Contents

Chapter 1

Self Propulsion

1.1 Motivation[5,6]

Figure 1.1: Ordered movement of ants

Figure 1.2: School of bluestrip snappers

Figure 1.3: A flock of starlings

In the discussion of physics in general, we usually omit one class of object which differ from all other objects in the universe by one peculiar property of *being alive*. Although we see a vast variety of these objects in the nature around us and even we belong to the same class as well! We are fascinated by the displays of collectively moving animals. We have seen the beauty of the patterns formed by orderly movement of school of fish or ant or birds. The pattern that flocks of hundreds of starlings make while flying are immensely beautiful. But they break the pattern when they return to their roosting site producing turbulent and puzzling and apparently chaotic aerial display. Schools of fish also show a orderly and uniform motion. That same fish can swirl like a intensely stirred fluid in presence of predators. These are a few examples of the rich behavior that we see in the animal kingdom. They differ from an inert lump of mass in the perspective that the living beings can do their own dynamics exploiting their own energy, this is the essence of self propulsion. The ability to move on their own (unlike the dead) and the ability to interact between themselves leads to a very rich dynamical behaviour as a consequence of self propulsion and collective behaviour. The dynamics that a group of living (or *active*) entity show is significantly different than a singular one. The interaction between them leads to *collective motion*, one of the conspicuous features of life. Perhaps the phrase *"More is different"*[3] which P.W Anderson used in a different context can be used in the case of collective behaviours too.

Apart from living beings, the features of self propulsion and collective motion can be found in several non-living systems too. It was successfully demonstrated that several non-living systems can be made to have these characteristics of self propulsion.

1.2 Active system

A kind of system which can propel on their own without any external influence is referred to as active matter. These systems possess some kind of internal driving mechanism which allows them to move autonomously. The driving mechanism that leads the system to be active may have different origins. This can be chemical reaction in case of living systems. For artificially driven systems, the active force can be originated from some non-equilibrium dynamics. This type of motion is different than passive motion of molecules in fluids. There exist an internal motors which takes in energy from environment and transfers it to kinetic degrees of freedom which leads the system to directed accelerated motion under non-equilibrium conditions. This kind of motion can be attributed to either an internal energy depot or a non-linear velocity dependent frictional force.

Another important feature of this class of system is the presence of non-negligible random fluctuations or "noise" in the motion of each individual units. This is mainly due to the smallness of the constituents of each individual units of the system. The source of the noise appearing in the dynamics may be due to fluctuations in the environment (say, the system is immersed in a heat bath) or it may be a inherent feature of the internal processes which generates the active forces. Whatever be the source, it is usually modelled by introducing a stochastic force term in the equations of motion, without taking the actual physical source into consideration.

An important properties of this stochastic force is that the time scales in which this force fluctuates is much smaller than the time scales in which the dynamical observables of the system in question, change. Along with the presence of a viscous force,this has the characteristics of a Brownian particle which is undergoing active motion. Thus most self propelled systems can be modelled using the concept of an Active Brownian Particle.

1.3 Modelling Active systems

1.3.1 Vicsek Model[4]

The earliest model for active Brownian particles was proposed by Vicsek et al. The basic idea is: At each timestep, each particle moves in the average direction of motion of its neighbors, plus some noise. Say that at $t = 0$, all N particles are randomly distributed in position and direction. Then we update the position and velocities with:

$$r_{i+1}(t) = r_i(t) + v_i(t)\Delta t \tag{1.1}$$

$$v_i(t) = v_0(\hat{x}cos(\theta_i) + \hat{y}sin(\theta_i)); |v_i| = v_0 \tag{1.2}$$

The heading directions are updated with

$$\theta_i(t + \Delta t) = arg[\sum_k e^{i\theta_k(t)}] + \xi(i, t) \tag{1.3}$$

which is the mean heading angle of particles in vicinity of the i-th particle. And $\sum_k$ is restricted by $|r_k - r_i| < R$ and ξ is a random noise $(-\pi, \pi]$

1.3.2 Rayleigh-Helmholtz Model[5]

In this model the activity is introduced by a velocity dependent force $F(v)$. The EOM reads

$$\dot{x} = v; \quad \dot{v} = -\gamma v + \eta(t) + F(v) - \partial_x U + f(t) \tag{1.4}$$

Within Rayleigh-Helmholtz model, one takes $F(v) = av - bv^3$ with $a > \gamma$. At small velocities $v < v_0$, velocity dependent force $g(v) = F(v) - \gamma v = b(v_0^2 - v^2)v$ pumps energy into kinetic degrees of freedom and generates self propulsion.

This model has been successfully used to analyze the motion of microtubule interacting with NK11 motor-proteins that generates energy by utilizing the chemical fuel of ATP.

1.3.3   Model by Hagan & Marchetti[1]

We have used this model model in our study which we'll describe in detail in chapter 5.

Chapter 2

Brownian Motion

2.1 Historical Background[4, 13]

In 1827, Robert Brown, an English botanist, observed under a microscope that pollen grains in water were in a constant state of agitation. He first thought that it might be something 'alive', but proved that was not so by observing the same kind of motion in inclusions in million years old quartz. He was not able to explain the observations.

Brownian motion, this seemingly simple phenomena gave rise to many puzzles that took almost 300 years to fully resolve. Brownian motion is one of the pathway through which one can start describing non-equilibrium systems. Historically it is of immense importance as it played a crucial role to firmly establish the existence of atoms closing an age old debate on the fundamental constituents of matter. Greek philosophers like Democritus, Leucippus assumed discrete constituent of matter, which was later postulated by Dalton. At the end of nineteenth century, the success of kinetic theory of gas developed by Maxwell, Clausius and Boltzmann was in favour of that idea. On the other hand Ernst Mach, Ostwald etc. strongly opposed the idea.

The first ever explanation to Brownian motion was given by Einstein in one of his three 1905 papers. Later J. Perrin experimentally verified Einstein's theory in 1926, for which he got the Noble prize.

2.2 Einstein's explanation[11]

Einstein described Brownian Motion in the following manner in one of the three pioneering papers that he published in 1905:

1. The movement of Brownian particles are caused by collisions of the molecules of the solvent. The fluctuating motion of the molecules are caused by their thermal energy.

2. The motion of the molecules is complicated and its effect on the motion of the pollen grains can be described as very frequent, statistically independent impacts on the particles.

The assumption underlying the above is that the collisions between any two particles, and the collisions occuring between two particles at different times, given that the time interval is large enough; are independent. The x-coordinate of each particle undergoes an increment of δ at some later instant of time. The value of δ can be positive or negative, but its values must follow a probability distribution $\phi(\delta)$ which has the characteristics that

$\phi(\delta) = \phi(-\delta)$ and $\int_{-\infty}^{\infty} \phi(\delta)d\delta = 1$. Thus the number of particles at time $t + \tau$ found between x and $x + dx$ is,

$$f(x, t + \tau)dx = dx \int_{\infty}^{\infty} f(x + \delta, t)\phi(\delta)d\delta \tag{2.1}$$

This is known as the Chapman-Kolmogorov equation. In effect, it states that the probability of finding a particle at a position x at a time $t + \tau$ is the sum of the transition probabilites of particles at all possible positions $x + \delta$ to be pushed to the position x multiplied by the probability of being at the position $x + \delta$ in the first place. This assumption is Markovian as it is essential that the push δ is independent of the previous collisions undergone by the particle. Assuming that the time interval τ and the space interval δ are very small, we have

$$f(x, t) + \tau \frac{\partial f}{\partial t} = f(x, t) \int_{-\infty}^{\infty} \phi(\delta)d\delta + \frac{\partial f}{\partial x} \int_{-\infty}^{+\infty} \delta \phi(\delta)d\delta + \frac{\partial^2 f}{\partial x^2} \int_{-\infty}^{+\infty} \frac{\delta^2}{2}\phi(\delta)d\delta + \text{higher order terms} \tag{2.2}$$

The above equation is known as Kramers-Moyal expansion. Using the properties of $\phi(\delta)$ and setting

$$\frac{1}{\tau} \int_{-\infty}^{+\infty} \frac{\delta^2}{2}\phi(\delta)d\delta = D_0 \tag{2.3}$$

Where, D_0 is the equilibrium diffusion constant and finally we get the diffusion equation,

$$\frac{\partial f}{\partial t} = D_0 \frac{\partial^2 f}{\partial x^2} \tag{2.4}$$

Einstein concluded by finding the rms displacement as

$$\langle x^2 \rangle = 2D_0 t \tag{2.5}$$

2.3 Langevin's description[4, 12]

The motion of a Brownian particle subject to Stokes friction with coefficient γ in presence of a external force $F(r) = -\nabla V(r)$ can be described by the following equation known as Langevin equation

$$\frac{d\mathbf{r}}{dt} = \mathbf{v}; \quad m\frac{d\mathbf{v}}{dt} = -\gamma v - \nabla U(\mathbf{r}) + \eta(t) \tag{2.6}$$

Where this $\eta(t)$ is again a delta correlated Gaussian white noise with

$$\langle \eta(t) \rangle = 0; \quad \langle \eta_i(t)\eta_j(t') \rangle = 2D_p \delta_{ij}\delta(t - t') \tag{2.7}$$

A stationary Wiener process is obtained by integrating η over small time interval dt. These fluctuating forces yield an increment of momentum in dt with Gaussian distribution with zero mean and with standard deviation (second moment) growing linearly with t at a rate of $2D_p$.

$$dW_{dt,i} = \int_t^{t+dt} ds\eta_i(s), \quad i = x, y, z \tag{2.8}$$

We may write Langevin equation in the following form

$$\frac{d\mathbf{r}}{dt} = \mathbf{v}; \quad \frac{d\mathbf{v}}{dt} = -\frac{\gamma}{m}v - \frac{\nabla U(\mathbf{r})}{m} + \sqrt{2D}\xi(t) \tag{2.9}$$

For non-interacting Brownian particles, i.e. $\nabla U(\mathbf{r}) = 0$, the mean squared displacement $\langle \mathbf{r}^2(t) \rangle$ starting at $t = 0$ in equilibrium can be found by integrating eqn..

$$\langle \mathbf{r}^2(t) \rangle = 6 \frac{k_B T}{\gamma} \left(t - \frac{1}{\gamma}(1 - \exp(-\frac{\gamma}{m}t)) \right) \tag{2.10}$$

This expression shows a ballistic growth for times smaller than $t \leq 1/\gamma$ and a linear growth for $t \to \infty$.

$$\langle \mathbf{r}^2(t) \rangle = 2dD_{eff}t \tag{2.11}$$

where d is the dimension of the Brownian motion and the diffusion constant D_{eff} obeys Einstein's realtion

$$D_{eff} = \frac{k_B T}{\gamma} \tag{2.12}$$

So we recover the Einstein's relation starting from Langevin's recipe.

In this regard the Fokker-Planck equation answers the following question: What is the transition probability $P(r, v, t | r_0, v_0, t_0)$ to find the tagged particle at location r with velocity v at time t if started at r_0 with v_0 at initial time t_0. This transition probablity $P(r, v, t | r_0, v_0, t_0)$ follows the following equation known as the Fokker-Planck equation.

$$\frac{\partial P(r, v, t | r_0, v_0, t_0)}{\partial t} + v \frac{\partial P}{\partial r} + \nabla U(r) \frac{\partial P}{\partial v} = \frac{\partial}{\partial v} \left[\gamma v P + D \frac{\partial P}{\partial v} \right] \tag{2.13}$$

Chapter 3

Phase transitions

3.1 Introduction[8]

Phase transitions are one of the the most ubiquitous phenomena in nature which involves abrupt changes in measurable macroscopic properties of systems and are brought about by varying external parameters such as temperature or pressure.

These phenomena are described mathematically by non-analyticity of thermodynamic functions (Yang-Lee theory), which reflect the drastic changes that takes place in the system at a microscopic level.

The solid-fluid phase transition which takes place in 2D colloidal system, interacting by purely repulsive potential is known to be a continuous phase transition of Kosterlitz-Thouless type.

3.2 The XY model in 2D[8,9]

Let us consider the 2D XY model as our reference model. The model consists of planar rotors of unit length arranged on a two dimensional square lattice with the Hamiltonian given by

$$H = -J \sum_{\langle i,j \rangle} \mathbf{S_i} \cdot \mathbf{S_j} \tag{3.1}$$

The state of matter we have identified is as close as XY spins can get to order in $d = 2$, and is called quasi long-range order (QLRO). We neither have broken symmetry nor the long range correlations, but the correlations still decay very slowly with distance.

But the spin wave theory alone can not a mechanism for the destruction of QLRO irrespective of how high is the temperature. This seems to be odd from what we expect, since we expect exponentially decaying correlations and only short range order at high temperatures $(T >> J)$, .

It was first realized by Berezinskii (1971), and then examined in detail by Kosterlitz and Thouless (1973) that, in the 2D XY model we can identify vortex configurations where the spins field is smooth everywhere except in a small region of space. The slowly decaying correlations in the spin phase $\theta(\mathbf{x})$ is eliminated in presence of these topological defects. To be more precise, let us define the "topological charge" of a vortex.

As all physical quantities (e.g. the energy) is a periodic function of the spin phase θ with period 2π, the topological charge must be an integer $n = 0, \pm 1, \pm 2, \pm 3, \cdots$.
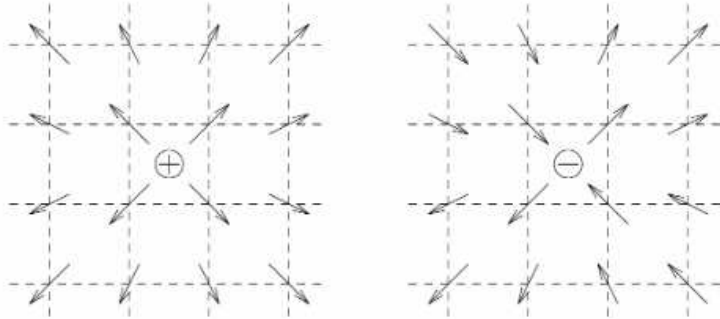

Figure 3.1: Vortex configurations characterized by topological charge $n = +1$ (left) and $n = -1$ (right)

Since the presence of a vortex rotates the phase over large distances, randomly placed vortices will completely scramble the phase, leading to short range order. In contrast, if a vortex and an antivortex pair are close to each other, the phase accumulated over a loop enclosing both of them vanishes. Depending how they are distributed in the system, the vortices may or may not destroy QLRO,

The energy of an isolated vortex can be shown to be

$$\beta E_n = \beta E_n^0 + \frac{n^2 \pi}{g} ln(\frac{L}{a}) \tag{3.2}$$

Clearly, the vortices with $n = \pm 1$ cost least energy, and will thus be most abundant.

3.3 Berezinskii-Kosterlitz-Thouless (BKT) transition

Here we present a heuristic argument to estimate how many vortices can be present at a given temperature.

The entropy of creating a single vortex is

$$S_n = 2ln\left(\frac{L}{a}\right) \tag{3.3}$$

And the free energy of creating a $n = \pm 1$ vortex is

$$\beta F_{\pm 1} = \beta E_{\pm 1}^0 + \frac{\pi}{g} ln\left(\frac{L}{a}\right) - 2ln\left(\frac{L}{a}\right) \tag{3.4}$$

As we can see from this expression, the first term is a finite number, whereas the last two both diverge logarithmically in the thermodynamic limit $L \to \infty$. The entropy will win and a finite concentration of free vortices will be created if

$$g > g_c = \frac{\pi}{2} \tag{3.5}$$

We therefore expect the vortices to proliferate above the Kosterlitz-Thouless temperature
$T_K T \sim g_c$, and the QLRO state to be destroyed.

3.4   Vortex unbinding[8]

The vortex-binding scenario is crucial to the BKT phase transition in the 2D XY model. The energy of a single vortex increases with the system size as $ln(L)$. Thus at low temperature they can only occur in vortex-antivortex pairs. Mutual cancellation of their individual ordering cannot significantly disorder the whole system. At low temperature topological long-range order does exist in the system . However at high temperature, the number of vortices proliferates and the distance between erstwhile partners becomes so large that they are effectively free and make the system disordered.
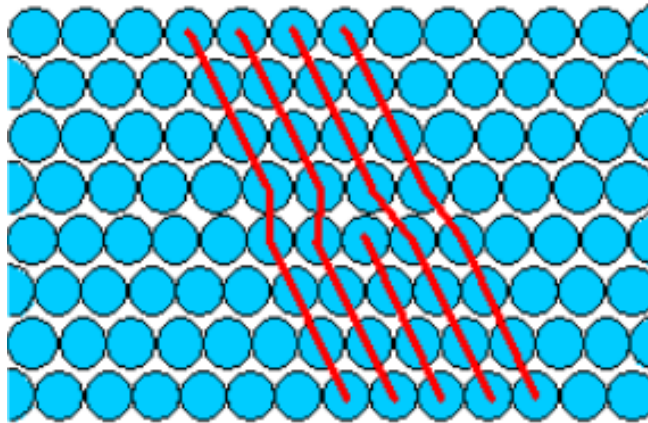
3.5   KT Transition in other systems

Figure 3.2: Dislocation in 2D crystal

Many other two dimensional systems display phase transitions that belong to the Kosterlitz-Thouless universality class. In all these cases, the phase transition is Dislocation in a 2D crystal driven by unbinding of topological defects.

3.6   Phase separation dynamics in active systems[10]

Whatever we have discussed so far are applicable for passive systems. Recently Lowen et al.[10] have derived an effective Cahn-Hilliard equation for the phase separation dynamics of active Brownian particles by performing a weakly non-linear analysis of the effective hydrodynamic equations for density and polarization.

Chapter 4

Molecular Dynamics Simulation

4.1 About Molecular Dynamics[17]

Molecular dynamics (MD) is a computer simulation technique which computes the time evolution of a set of interacting particles by numerically integrating their equations of motion. The technique has been applied to systems of several hundreds to millions of particles and has given much information about the behaviour of interacting classical many-particle systems. The physical movements of atoms and molecules are investigated by numerically solving Newton's equation of motion using a description for the inter-atomic interaction. Equilibrium and transport properties are obtained using the approach developed within statistical mechanics.

The method was originally conceived within theoretical physics in the late 1950s. Now it is applied extensively in various scientific disciplines as materials and nano-sciences, and for biomolecular systems.

A typical MD simulation follows the following steps

1. **Initialisation:** At $t = 0$, an initial lattice is generated and particles are placed accordingly.

2. **Interaction forces:** Interaction forces ($F_i = \sum_{j \neq i} F_{ij}$) on each of the particles is calculated.

3. **Integration of EOMs:** Given the interaction forces $\mathbf{F}(\mathbf{r_i})$ the EOMs are integrated. Verlet, velocity Verlet integration schemes are generally used.

4. $t = t + \delta t$

5. Step # 2 to 4 are repeated until required time $t = t_{max}$ is reached.

4.2 Techniques for Saving CPU Time

The most time consuming part in any MD simulation is computation of interaction forces as it scales as $O(N^2)$ which makes the MD program quite inefficient. For a system of N particles, calculation of interaction force on a particle requires an evaluation of $N(N-1)/2$ particle pairs. There are a few tricks that is generally used to reduce it.
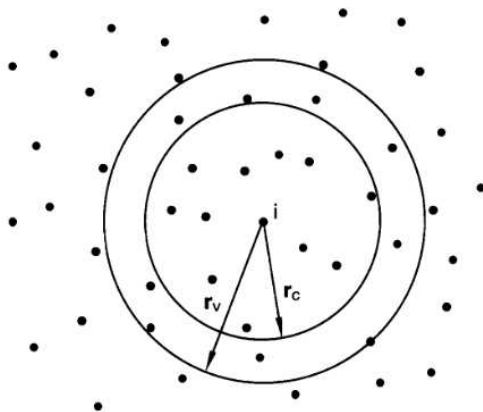
Figure 4.1: The Verlet list scheme: the i-th particle interacts with those particle which falls within the sphere of radius r_c and the Verlet list of i-th particle contains all the particles within the sphere with radius $r_v > r_c$.[14]

4.2.1 Verlet List[14, 15]

The idea of Verlet list is based on the fact that if we simulate a large system and use a cutoff smaller than the simulation box, only a few particles out of total $(N-1)$ particles interacts with a particle. So it is advantageous to exclude the particles that do not interact from the computationally expensive energy calculation. In this method a second cutoff radius $r_v > r_c$ is introduced and a list of neighbouring particles which falls in the cutoff radius r_v is made for all the particles in the system. Now for subsequent force calculations, we need not to consider all $N(N-1)/2$ pairs, it is enough to consider the particles in the Verlet list if the displacements of the particles are less than $r_v - r_c$. So we update the Verlet list if any of the particles moves beyond $r_v - r_c$. Though updating the Verlet list is still a $O(N^2)$ operation but on the long run we save CPU time as it the Verlet list need not to be updated frequently, typically once in every 10-20 steps.
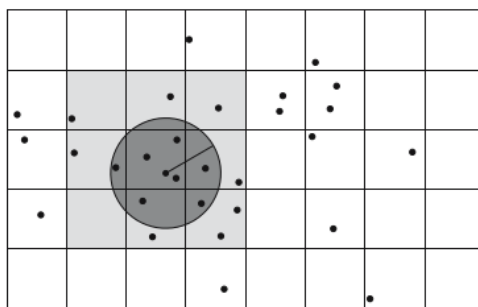
4.2.2 Cell List[16, 18]

Figure 4.2: Cell list scheme: The dark-shaded area shows the domain of influence of a particle with a cutoff radius r_c . So to calculate interaction force on that particle we need to scan all the particles in the neghibouring 8 cells.[16]

The Verlet list scheme becomes inefficient for large system, typically for number of particles exceeding a few thousands. For such a system generally the Cell list or the Linked list approach is preferred. In this method the simulation box is subdivided into "cells" of dimension $r_c \times r_c$. Initially a cell list is generated which distributes the particles in respective cells according to their positions. Now a particle in a certain cell will only interact with the particles which lie in its neghibouring cells, thus we no more need to scan over $N(N-1)/2$ number of

particle pairs. In this way the force calculation part is reduced to $O(N)$ process. After each integration step the cell list is accordingly updated with new particle positions which is anyway a $O(N)$ operation. So the computational complexity of the problem is linearised in cell list method.

A cell has respectively 8 and 27 neghibours in two and three dimensions. For a system of particles where Newton's third law holds, i.e. $F(\mathbf{r_{ij}}) = -F(\mathbf{r_{ji}})$, only half of the neighbouring cells need to be traversed. Thus it makes the scheme more efficient.

4.3   Parallel Molecular Dynamics[16]

To take the full advantages of modern computers and clusters with multiple CPUs and cores, we need to *parallelize* the MD routine. We list the possible methods with their complexities for short range forces. Here N is the number of particles and P is the number of processors.

Parallalization strategy	computation complexity	communication complexity	memory requirements per processor
replicated data	$O(N/P)$	$O(N)$	$O(N)$
data partitioning	$O(N/P)$	$O(N/P)$	$O(N/P)$
domain decomposition	$O(N/P)$	$O(\sqrt{N/P})$ in 2D	$O(N/P)$

Out of these three the domain decomposition method is the most efficient one as it has the least complexity in all operations, specially it needs least amount of data transfer between processors.

In this method the whole simulation domain is divided into a number of subdomains and is assigned to available processors. Now each of these processors contains information of the particles of their respective subdomain. Each of these subdomains are further subdivided into cells as in the sequential cell list method.
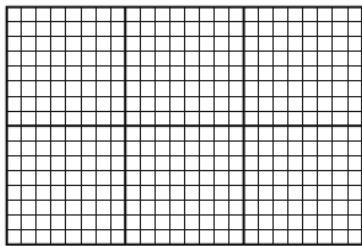

Figure 4.3: Here we subdivided the simulation domain into 6 small subdomains which are owned by 6 different processors. These subdomains are further divided into cells as in the sequential cell list method
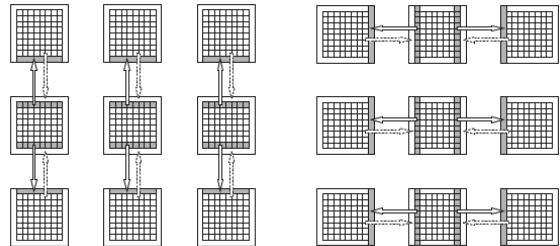

Figure 4.4: Data must be exchanged in between neghibouring processors in order to correctly calculate interaction forces on particles which lie in subdomain boundaries. This figure depicts the transfer pattern and *ghost* cells which are useful in this kind of *halo* exchanges.

For calculating interaction forces of the particles in the boundary cells, particles which belong to the boundary cells of neghibouring subdomains must the communicated among the processors. This is termed as *halo* transfer. Then all the processors parallely calculate interaction forces and integrates the equation of motion of the particles belonging to them. After this step the particles that came in or moved out from their own subdomain must be exchanged according to their updated positions.

The data exchange among processors can be easily handled by Message Passing Interface (MPI), a standardized and portable message-passing system designed by a group of researchers from academia and industry to function on a wide variety of parallel computers.

Using the same parallelization strategy, MD problems can be parallalized in Graphics Processing Units (GPU) instead of CPUs as well. In this case nVidia CUDA^{TM}(a proprietary software available for nVidia GPUs) or OpenCL (an open standard, implementated by most of the GPU and CPU vendors) can be very useful.

For our simulation we have parallalised the MD problem by using this domain decomposition method and we have used MPICH (an open implementation of MPI) for data exchanges.

Chapter 5

Our Model and Simulation

5.1 Our model

The model we are using here was proposed by Merchetti et. al.[1,2]

In this model we consider a system of self-propelled smooth spheres interacting by excluded volume. These particles can not interchange angular momentum and so there is no mutual alignment mechanism.

The state of the system is defined by the positions and self-propulsion directions $\{\mathbf{r_i}, \theta\}_i^N$ of all the N number of particles. The time evolution of the particles is governed by the coupled overdamped Langevin equations, i.e.

$$\dot{\mathbf{r_i}} = D\beta[-\nabla V_{ex}(\{\mathbf{r_i}\}) + F_p\hat{\mathbf{v_i}}] + \sqrt{2D}\eta_{\mathbf{i}}^{\mathbf{T}} \tag{5.1}$$

$$\dot{\theta} = \sqrt{2D_r}\eta_i^R \tag{5.2}$$

The $V_{ex}(\{\mathbf{r_i}\})$ in the radial coordinate is given by the WCA potential, i.e.

$$V_{ex} = 4\epsilon\left[\left(\frac{\sigma}{r}\right)^{12} - \left(\frac{\sigma}{r}\right)^6\right] + \epsilon \text{ if } r < 2^{\frac{1}{6}}$$
$$= 0 \text{ otherwise.} \tag{5.3}$$

here σ is the nominal particle diameter and we used $\epsilon = k_B T$.

F_p is the magnitude of the self-propulsion force. In absence of interaction forces, the self-propulsion force will move a particle with speed $v_p = D\beta F_p$. Direction of the self-propulsion is $\hat{\mathbf{v_i}} = \hat{\mathbf{x}}cos(\theta_i) + \hat{\mathbf{y}}sin(\theta_i)$. θ_i is the heading angle of the i-th particle.

D and D_r are translational and rotational diffusion constants, which are related by $D_r = \frac{3D}{\sigma^2}$ in the low Reynolds number regime.

The η are Gaussian delta correlated noise variables, i.e.

$$\langle \eta_i(t) \rangle = 0 \tag{5.4}$$

$$\langle \eta_i(t)\eta_j(t') \rangle = \delta_{ij}\delta(t - t')$$

Parameters We parameterised the system with system density ρ and Peclet number Pe. We nondiamensionalized the equation of motion by taking σ and $k_B T$ as basic units of length and energy and $\tau = \frac{\sigma}{D}$ as unit of time. We nondiamensionalized the propulsion speed v_p by introducing a diamensionless quantity *Peclet number* Pe $= v_p \frac{\tau}{\sigma}$. The Peclet number is a measure of activity of the system. That is, a higher Peclet number essentially means that the system is more active.

5.2 Simulation

We used 2D molecular dynamics simulation in overdamped limit (i.e. a so called *brownian dynamics* simulation) to find out various properties of the system.

Initial configuration We took a 2D simulation box with periodic boundaries, with its dimensions L_x and L_y chosen to attain desired system density for a given number of particles arranged in a triangular lattice.

If there are N_x & N_y number of particles along x & y axis respectively, then

$$L_x = a_x N_x$$

$$L_y = a_y N_y \tag{5.5}$$

$$\rho = \frac{N_x N_y}{L_x L_y} = \frac{1}{a_x a_y} \tag{5.6}$$

In triangular lattice

$$a_y = \frac{\sqrt{3}}{2} a_x \tag{5.7}$$

So that the system density can be expressed as

$$\rho = \frac{2}{\sqrt{3}a_x^2} \tag{5.8}$$

Numerical integration We integrated the equation of motion using stochastic Euler scheme. Lets take a Langevin equation

$$\dot{r} = D\beta F(r) + \sqrt{2D}\eta \tag{5.9}$$

We update the particle positions with

$$r(t + \Delta t) = r(t) + D\beta F(r, t)\Delta t + \xi(t) \tag{5.10}$$

Where ξ is a Gaussian random variable with $\langle \xi(t) \rangle = 0$ and $\langle \xi(t)\xi(t') \rangle = 2D\Delta t\delta(t - t')$.

We used a system of 4096 and 16384 particles with Peclet number 10,50,90 and 150. We simulated the system for $2 \times 10^6 \delta t$ time with $\delta t = 1 \times 10^{-5}$. We waited for first $1 \times 10^6 \delta t$ for the system to reach a steady state. Over the next $1 \times 10^6 \delta t$ time we sampled data at regular interval and analysed them.

Chapter 6

Results

6.1 Unconfined System

6.1.1 Snapshots of configuration

Here we present the snapshots of the system configuration at steady state with their corresponding distribution of local density at different Peclet numbers. To calculate the local density, we divided the system in suitable number of cells of fixed dimensions L_x & L_y and calculated the the number of particles in that cells. So, if there are N_i particles in i-th cell, then the local density in that cell would be $\rho_i = N_i/L_xL_y$.

Pe = 10
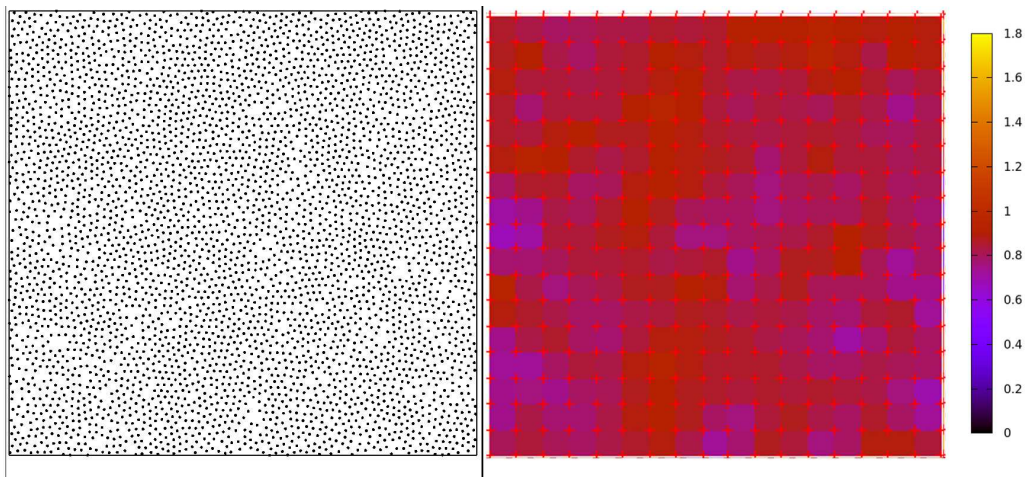
Figure 6.1: Snapshot of configuration (left) and local density (right) with parameters $N = 4096, \rho = 0.8$
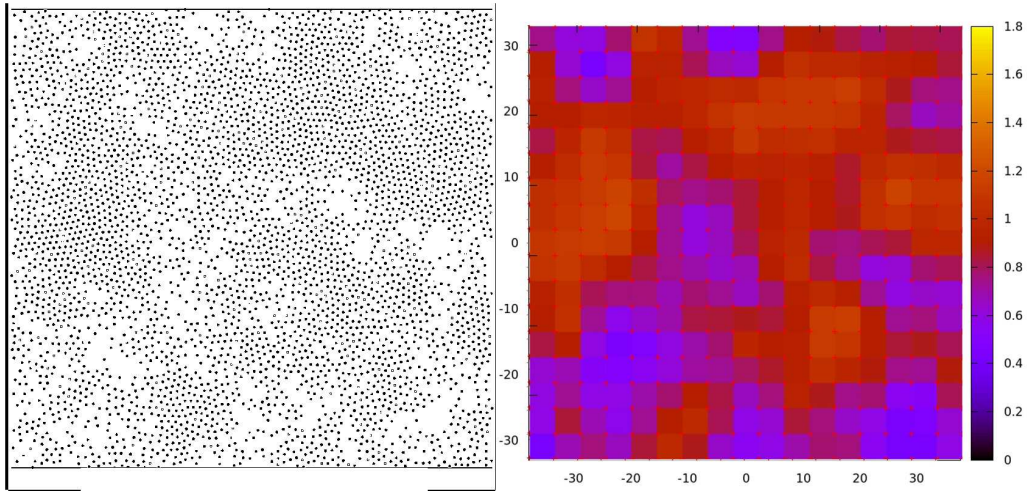
Pe = 50

Figure 6.2: Snapshot of configuration (left) and local density (right) with parameters $N = 4096, \rho = 0.8, Pe = 50$

Pe = 90
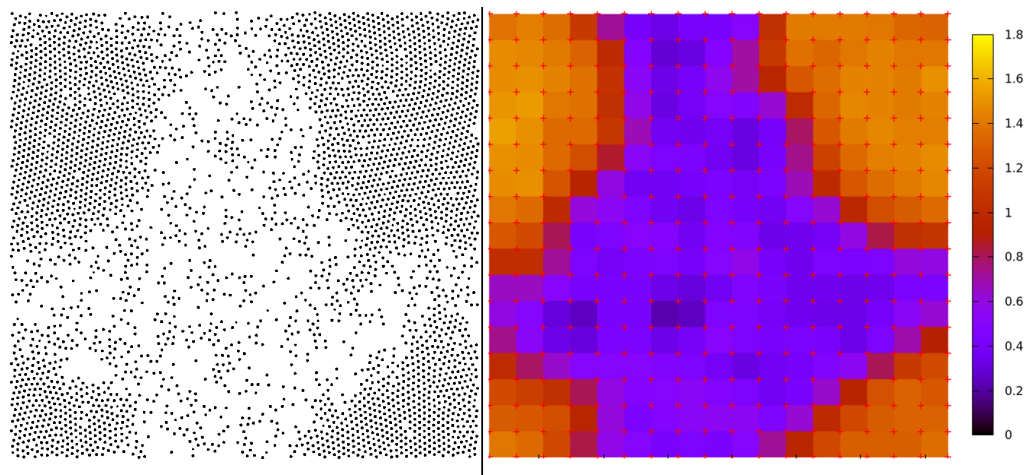
Figure 6.3: Snapshot of configuration (left) and local density (right) with parameters $N = 4096, \rho = 0.8, Pe = 90$

Pe = 100
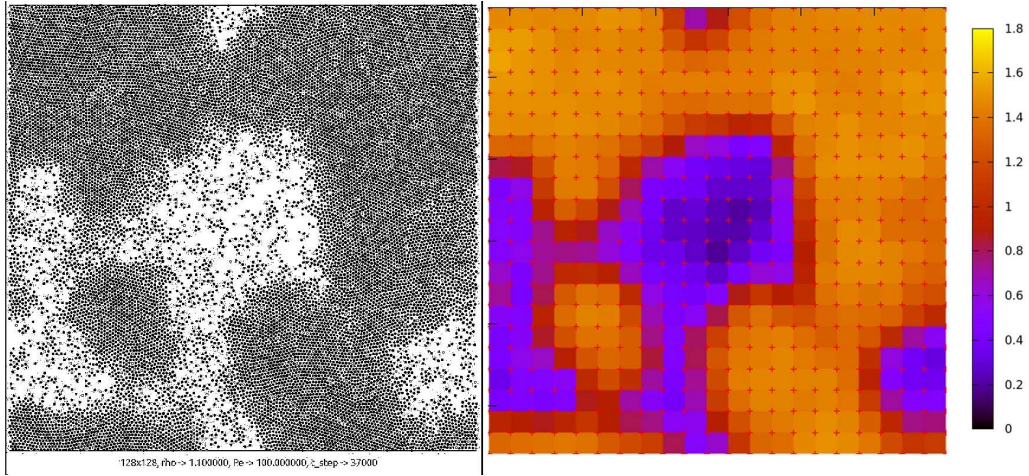
Figure 6.4: Snapshot of configuration (left) and local density (right) with parameters $N = 16384, \rho = 1.1, Pe = 100$
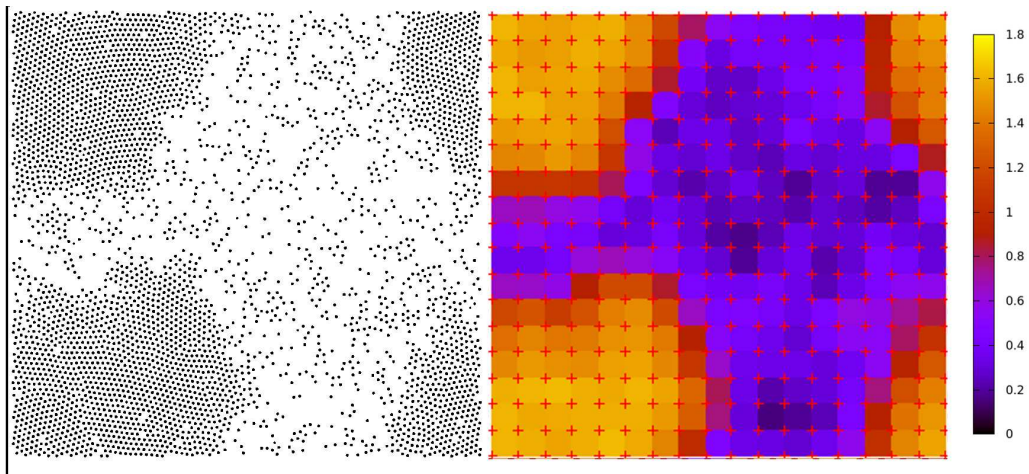
Pe = 150

Figure 6.5: Snapshot of configuration (left) and local density (right) with parameters $N = 4096, \rho = 0.8, Pe = 150$

6.1.2 Distribution of densities

Here we have plotted the probability distribution function of density $P(\rho)$. This shows co-existence of solid and fluid phase for higher Peclet number. This is a first order phase transition.[10]
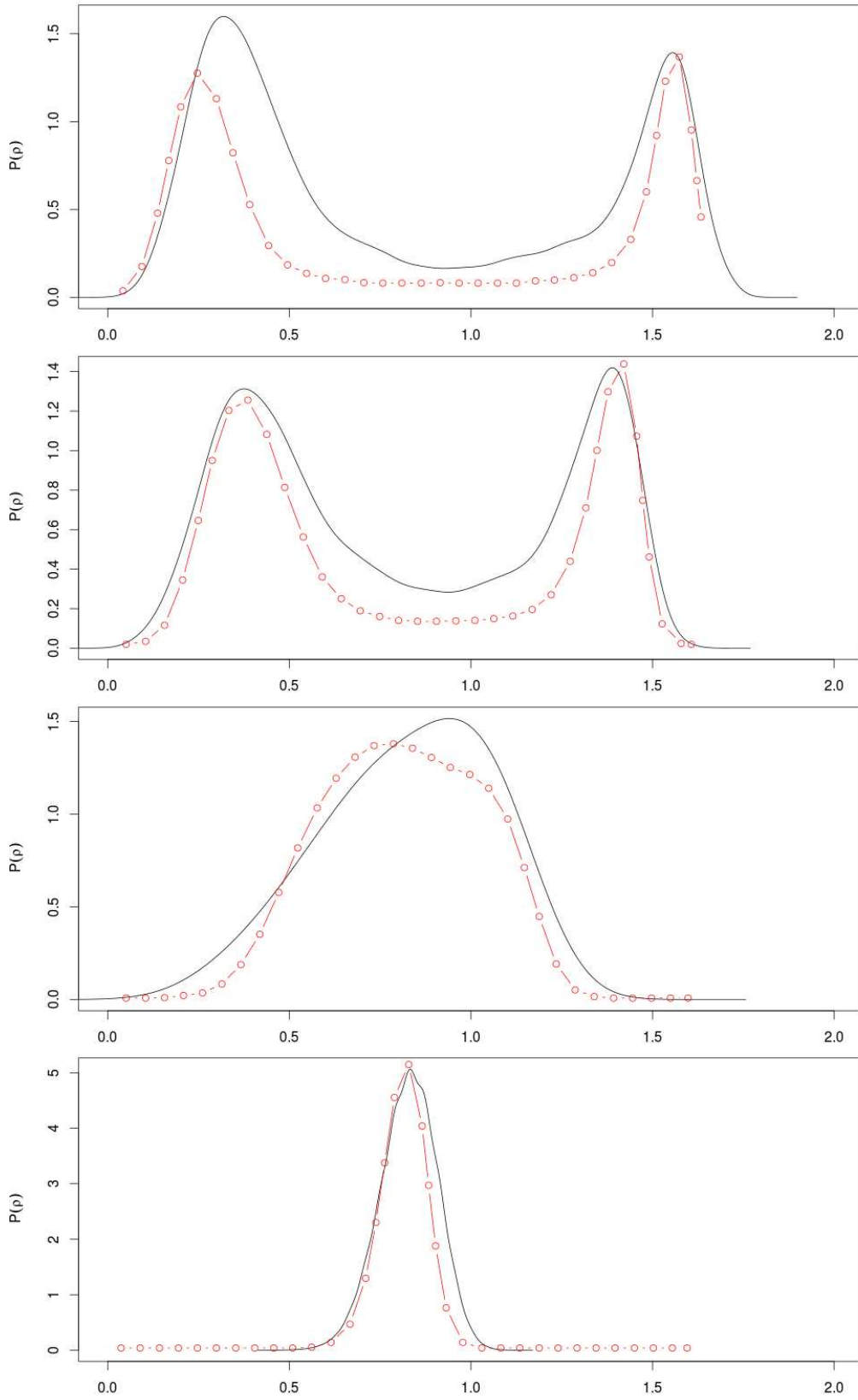
Figure 6.6: Distribution of probability of local densities $P(\rho)$ as a function of density ρ for Pe= $150, 90, 50, 10$ (from top to bottom). Solid lines are from our data and data marked with $\circ$ are previously published values[2]

6.1.3 Pair correlation functions $g(r)$ and $S(k)$

Radial distribution function $g(r)$ is defined as the ratio between the average number density $\rho(r)$ at a distance r from any given atom and the density at a distance r from an atom in an ideal gas at the same overall density.

The radial distribution $g(r)$ is one class of function that characterizes the local structure of a fluid thus it plays a crucial role in theories of liquid state. This is interesting because neutron and X-ray scattering experiments on simple fluids and light scattering experiments on colloidal suspensions, yield information about $g(r)$. Numerical results of $g(r)$ can be compared with theoretical predictions and experimentally obtained data. Thus it serves as a criterion to test a particular theory.

Another quantity of interest can be the static structure factor $S(\mathbf{k})$ defined as

$$S(\mathbf{k}) = \langle \rho_{\mathbf{k}} \rho_{-\mathbf{k}} \rangle \tag{6.1}$$

Where $\rho_{\mathbf{k}}$ is the Fourier component of the microscopic density $\rho(\mathbf{r})$ defined as

$$\rho(\mathbf{r}) = \sum_{i=1}^{N} \delta(\mathbf{r} - \mathbf{r}_i) \tag{6.2}$$

$$\rho_{\mathbf{k}} = \int \rho(\mathbf{r}) exp(-i\mathbf{k} \cdot \mathbf{r}) = \sum_{i=1}^{N} exp(-i\mathbf{k} \cdot \mathbf{r_i}) \tag{6.3}$$

$g(\mathbf{r})$ and $S(\mathbf{k})$ are related by

$$\mathbf{S}(\mathbf{k}) = 1 + \rho \int g(\mathbf{r}) exp(-i\mathbf{k} \cdot \mathbf{r}) d\mathbf{r} \tag{6.4}$$

Conversely, an inverse Fourier transform would yield

$$\rho g(\mathbf{r}) = (2\pi)^{-3} \int [\mathbf{S}(\mathbf{k}) - 1] exp(i\mathbf{k} \cdot \mathbf{r}) d\mathbf{k} \tag{6.5}$$
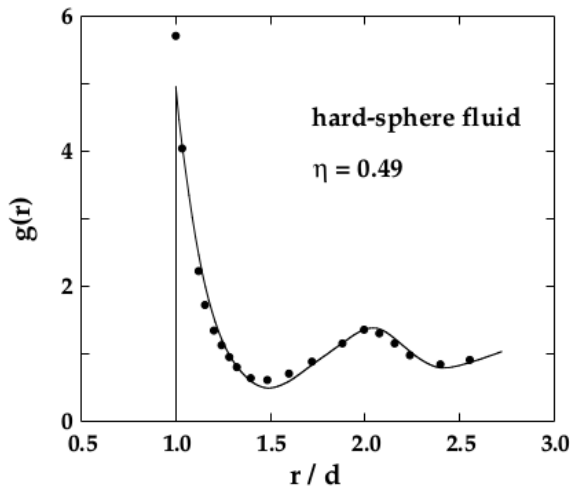

Figure 6.7: $g(r)$ for hard sphere fluid at a density close to liquid-solid phase transition
7

20

We have calculated $g(r)$ for our system at different Peclet numbers. The results are the following
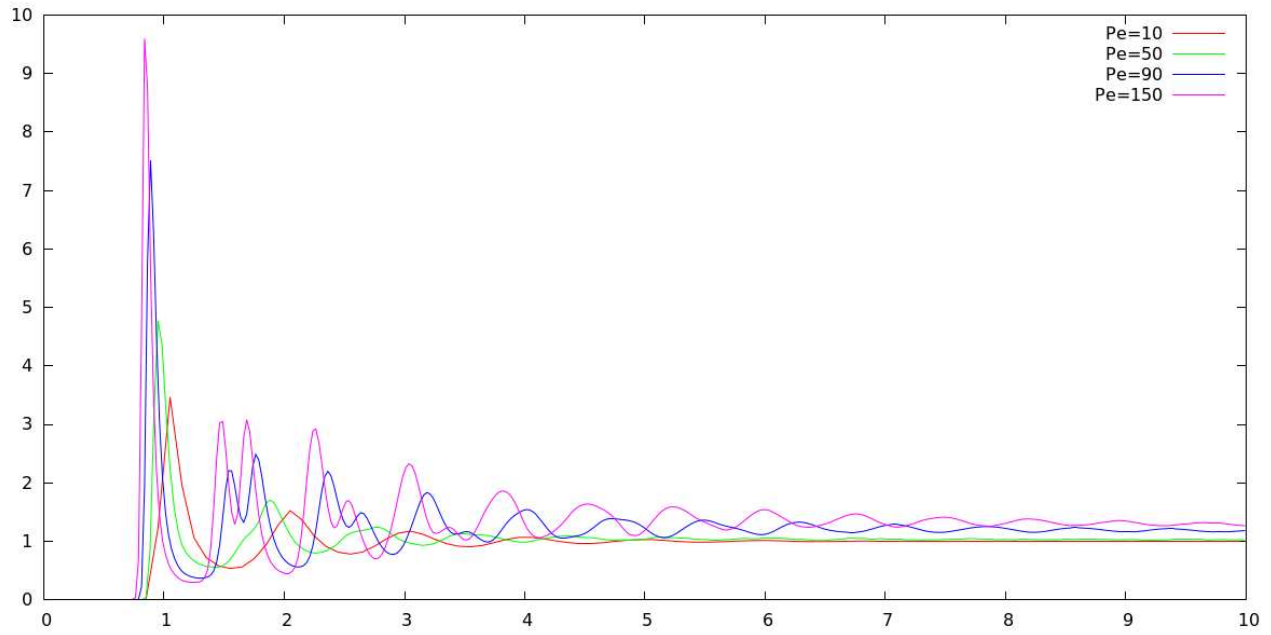

Figure 6.8: $g(r)$ for different Peclet numbers. Splitting of the second peak for Pe=90,150 characterizes a solid-fluid phase transition

6.1.4 Clustering Analysis

To find out structural properties of the two co-existing phases, we should analyse these two phases separately. This is done by clustering analysis.
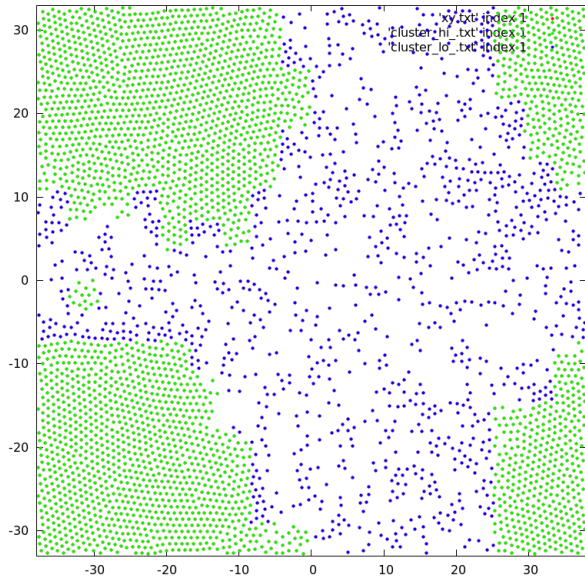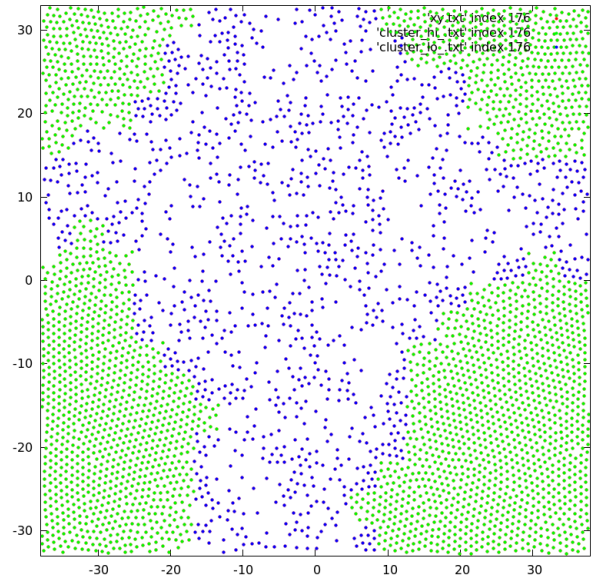

Figure 6.9: At Pe=150
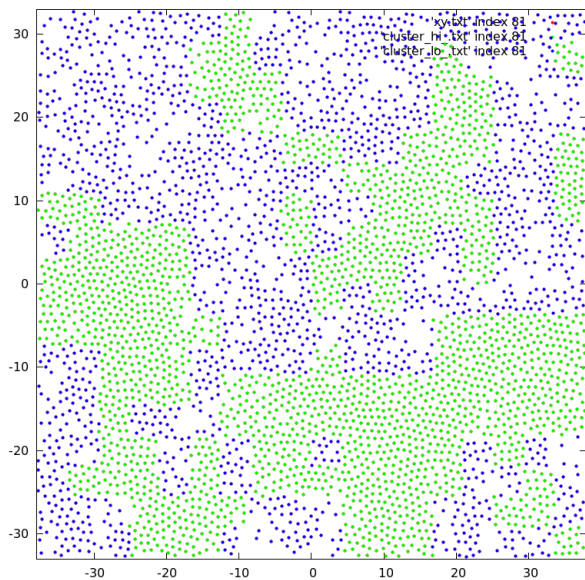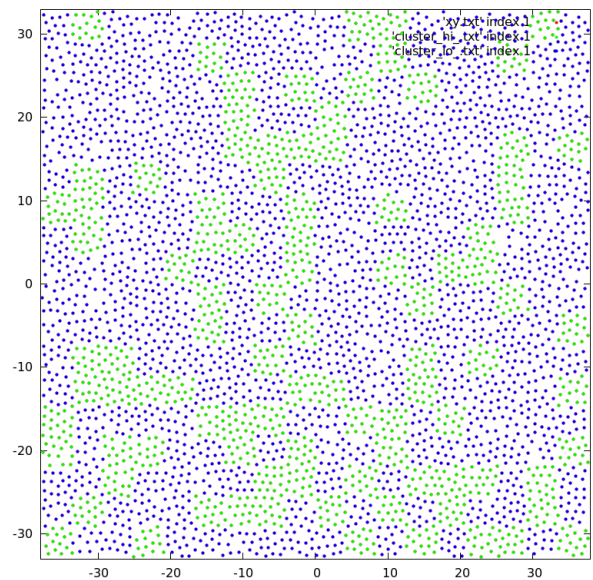

Figure 6.10: At Pe=90

Figure 6.11: At Pe=50

Figure 6.12: At Pe=10

Particles which are in high density phase (solid) are marked in green and those which are in low density phase (fluid) are marked in blue. We readily observe from the above clustering analysis that the amount of solid phase increases with increasing Peclet number, as we expected. At lower Peclet number we see very little or no solid phase at all. Now we'll calculate $g(r)$ at these solid and fluid phases separately.
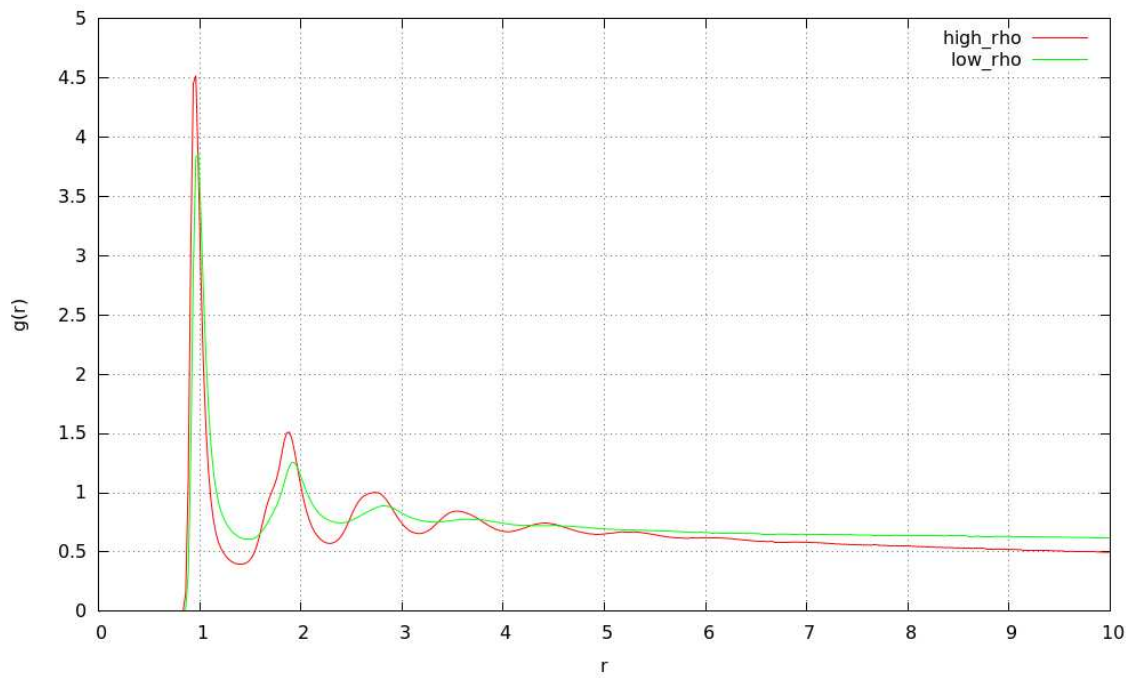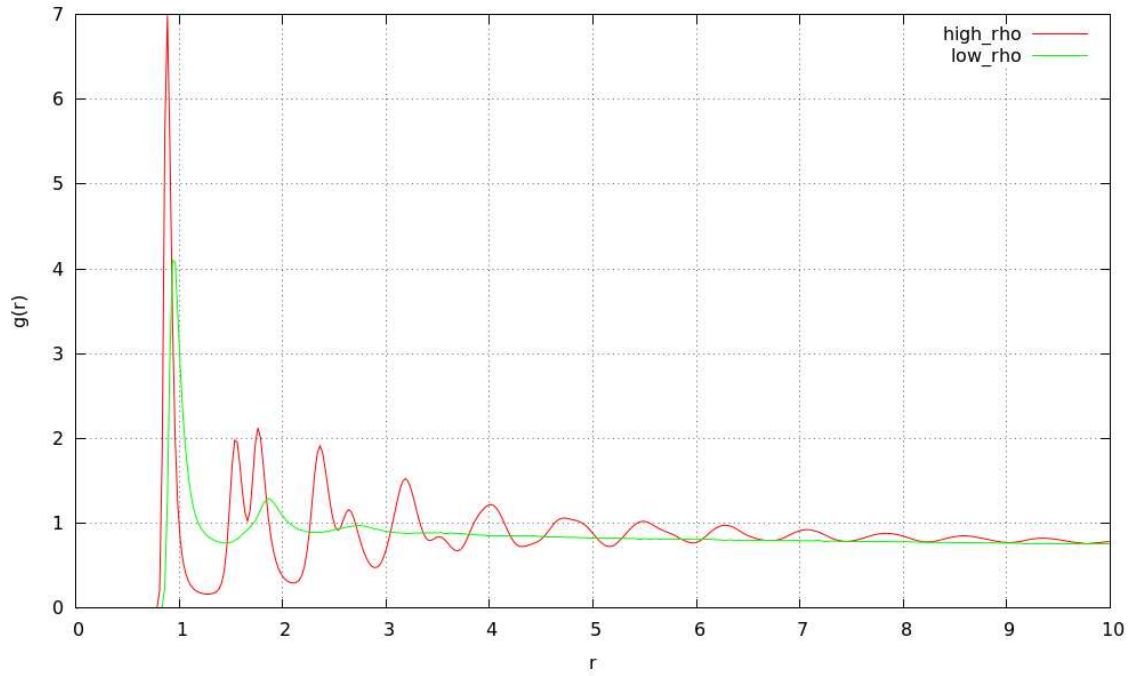
Figure 6.13: $g(r)$ for solid and fluid phases at Pe=90 (top) and for Pe=50 (bottom).[23]

6.2 Confined System

Now we replace the periodic boundaries in north and south direction by two static "walls". These walls produce a short ranged strong repulsive force on the particles. It was known[21] that confined active particles behave differently than confined passive particles.

When a gas of particles is placed in a confined environment such as a room or box, the particles can bounce off the wall creating a pressure. The system can readily be very well described by the ideal gas law $PV = nRT$, where P is the pressure, V is the volume, and T is the temperature. This means that if one increases the temperature at constant volume, the pressure will increase. Moreover, if the volume is fixed, the shape of the container has no effect on the pressure. One can picture an ideal gas by considering its particles as randomly walkers that explore all space in the container with equal probability. As the temperature increases, the particles diffuse faster.

All of these pictures can change if the particles are active or self-driven. Active systems undergo run-and-tumble dynamics and self-motile colloids that perform driven Brownian motion.[19, 20] The root mean square displacement of a single active particle exhibits superdiffusive or ballistic behavior at shorter times since the particles are effectively ballistically moving in a fixed direction. While at long times the particles exhibit diffusive behavior.[21]

6.2.1 Snapshots of configuration

In a active system under confinement, we see accumulation of the particles at the boundaries from our simulation. Thereby creating a solid phase near the boundaries and a fluid phase at the center. But it was shown that a passive system under confinement exhibits density modulation.[22]
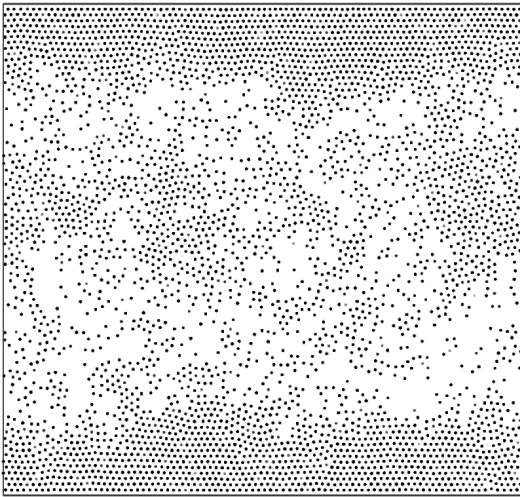

Figure 6.14: This snapshot of active particles under confinement shows accumulation of the particles near boundary.
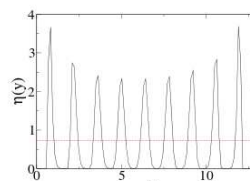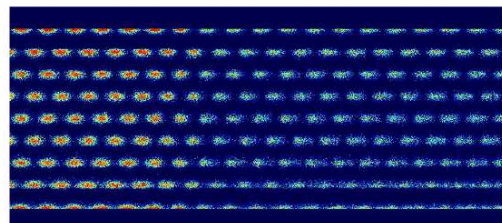

Figure 6.15: This shows that passive particles under confinement exhibits density modulation.[22]

6.2.2 Interface

We also traced the interface of solid and fluid phases for the confined active systems.
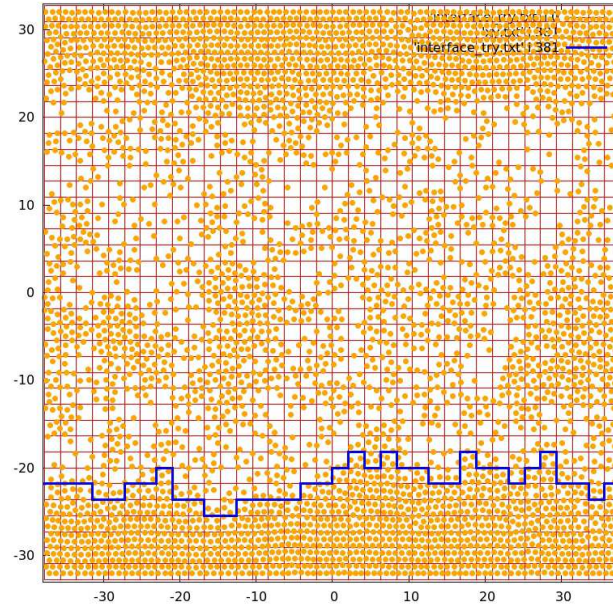

Figure 6.16: Tracing the solid-fluid interface in our confined active system.

Tracing the solid-fluid interface is crucial as we require it to understand the interfacial dynamics. We define the interface by the function $h(x, t)$ which is just the height of the interface from the confined boundary. Numerically we traced these boundaries by comparing local densities.

6.2.3 $h(x,t)$ autocorrelation

We have calculated the autocorrelation function $\langle h(x,t)h(x,0)\rangle$ from which the correlation time can be found which is essentially a measure of the time scale over which the quantity $h(x,t)$ remains correlated.

We have identified the solid-fluid interface at points $x_1, x_2, x_3 \cdots x_n$, i.e. we have $h(x_1,t), h(x_2,t), h(x_3,t) \cdots h(x_n,t)$. We have calculated $\langle h(x_i,t)h(x_i,0)\rangle$ for all i and then calculated the mean $\overline{\langle h(x,t)h(x,0)\rangle} = \frac{1}{n}\sum_{i=1}^{n}\langle h(x_i,t)h(x_i,0)\rangle$ and finally fitted the mean autocorrelation $\overline{\langle h(x,t)h(x,0)\rangle}$ with an exponentially decaying function $f(t) = a\exp(-t/t_c)$ where t_c is the correlation time. The best fit values are coming out to be $a = 0.872$ and $t_c = 5.74 \times 10^{-5}$.
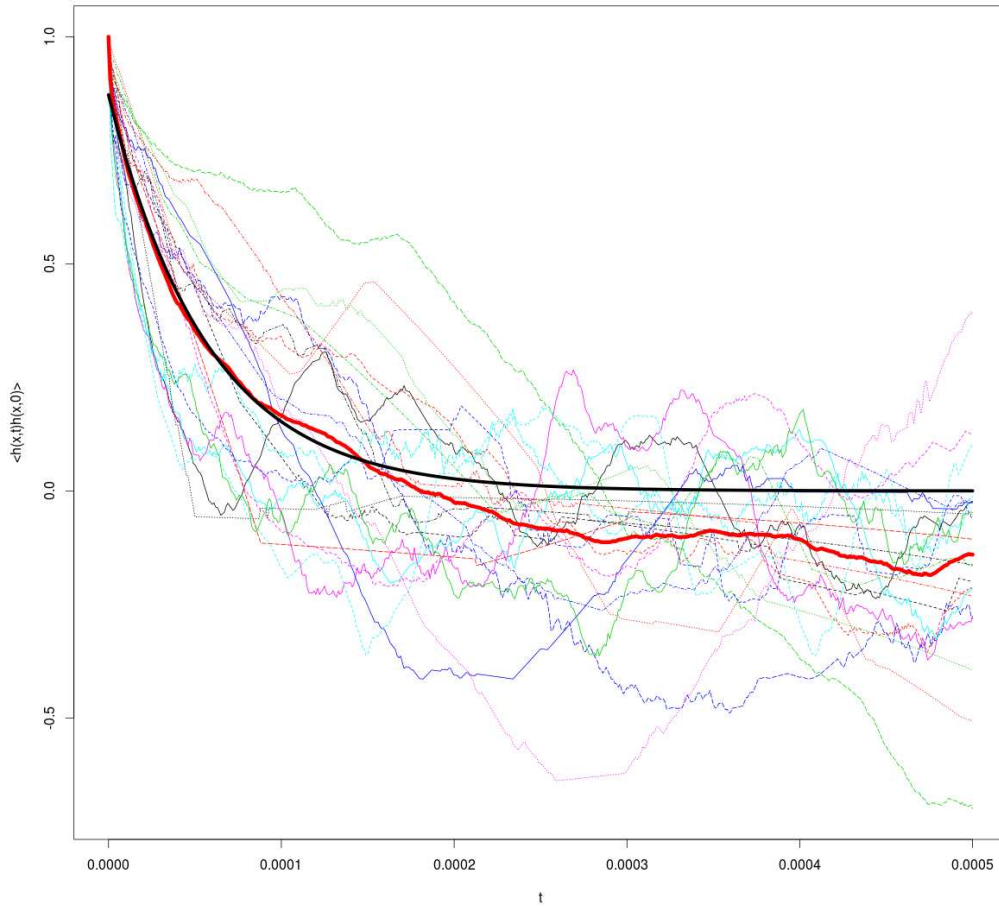

Figure 6.17: Plot of $h(x,t)$ autocorrelation. Here,
Faint dotted lines are the autocorrelation $\langle h(x_i,t)h(x_i,0)\rangle$ for $i = 1, 2, 3, \cdots$,
Thick red line is the mean autocorrelation $\overline{\langle h(x,t)h(x,0)\rangle} = \frac{1}{n}\sum_{i=1}^{n}\langle h(x_i,t)h(x_i,0)\rangle$,
Thick black line is the fit of $\overline{\langle h(x,t)h(x,0)\rangle}$ with $a\exp(-t/t_c)$.

6.2.4 Power Spectrum

We computed the power spectrum of $h(x_i, t)$, i.e. $\tilde{h}_i(\omega)$ for $i = 1, 2, 3, \cdots, n$. Then we computed the mean $\left\langle \tilde{h}_i(\omega) \right\rangle = \frac{1}{n} \sum_{i=1}^{n} \tilde{h}_i(\omega)$. We observed that $\left\langle \tilde{h}_i(\omega) \right\rangle$ fits well with $a\omega^{-1.5}$.
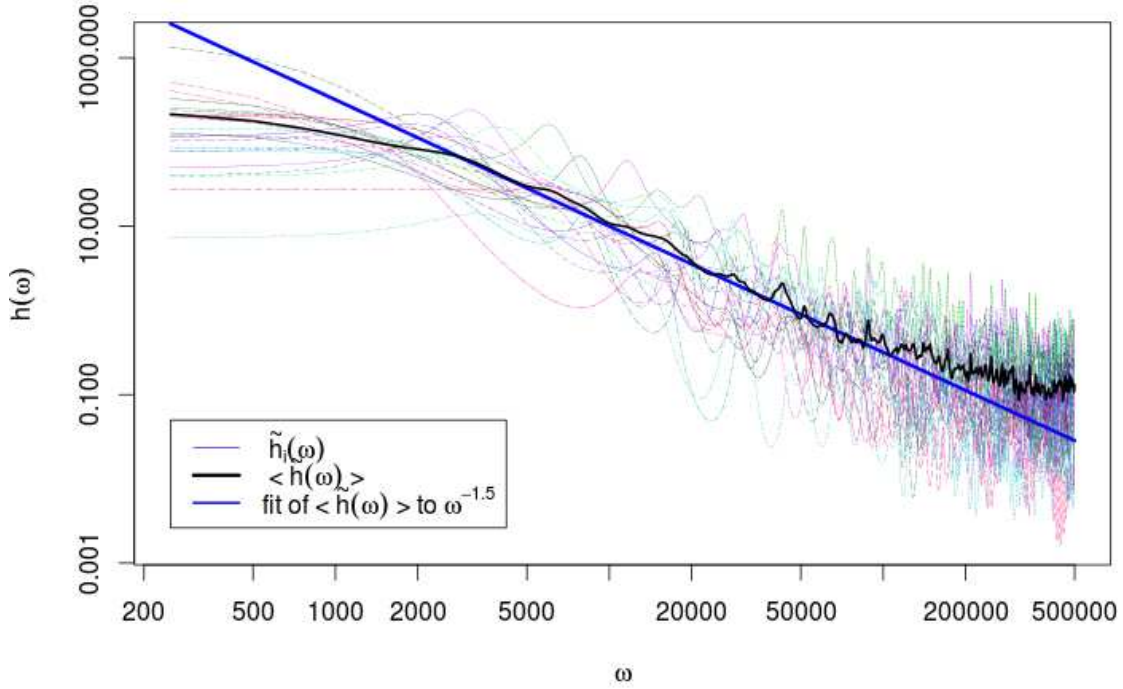

Figure 6.18: Power spectrum $\tilde{h}(\omega)$ Here,
Faint dotted lines are $\tilde{h}_i(\omega)$ for $i = 1, 2, 3, \cdots$,
Thick black line is the mean $\left\langle \tilde{h}_i(\omega) \right\rangle = \frac{1}{n} \sum_{i=1}^{n} \tilde{h}_i(\omega)$,
Thick blue line is the fit of $\left\langle \tilde{h}_i(\omega) \right\rangle$ with $a\omega^{-1.5}$.

6.3 Outlook

We end our work here by listing possible works that can be done in future:

1. Phase coexistence: what are equivalent quantities to thermodynamic forces in active systems?

2. Confined system: study the interfacial dynamics, two-time correlation.

3. To answer these questions: Critical fluctuations, Order of transition taking place in active systems and what could be the critical exponents etc. These are not known yet for active systems.

4. Extensions: Coupling of heading directions to local velocity fields. What happens as one changes coupling strengths?

References

[1] **Athermal Phase Separation of Self-Propelled Particles with no Alignment, Yaouen Fily, M. Cristina Marchetti**

[2] **Structure and Dynamics of a Phase-Separating Active Colloidal Fluid, Gabriel S. Redner, Michael F. Hagan, Aparna Baskaran**

[3] More Is Different, P. W. Anderson, Science, New Series, Vol. 177, No. 4047. (Aug. 4, 1972), pp. 393-396.

[4] Active Brownian Particles. From Individual to Collective Stochastic Dynamics, Romanczuk, Pawel Ebeling, Werner Lindner, Benjamin Schimansky-Geier, Lutz

[5] Active Brownian Particles: Entropy production and fluctuation-response, Debasish Chaudhuri

[6] Collective motion, Tamás Vicsek, Anna Zafeiris

[7] Theory of Simple Liquids, Hansen-McDonald

[8] The XY Model and the Berezinskii-Kosterlitz-Thouless Phase Transition, Ralph Kenna

[9] Vortices and the Berezinskii-Kosterlitz-Thouless Transition, PHY6938-01: Phase Transitions and Critical Phenomena Lecture Notes, Spring 2015, FLorida State University

[10] Dynamical mean-field theory and weakly non-linear analysis for the phase separation of active Brownian particles Thomas Speck, Andreas M. Menzel, Julian Bialke, and Hartmut Lowen

[11] Lecture notes on random walks and semiflexible polymers Part (I) : Statics by Abhishek Dhar, RRI

[12] Non equilibrium Statistical Mechanics by Robert Zwanzig

[13] 100 years of Einstein's theory of Brownian motion: from pollen grains to protein trains, Debasish Chaudhury

[14] Molecular Simulation, Frenkel and Smit

[15] Computer Simulation of Liquids, Allen Tildesly

[16] Numerical Simulation in Molecular Dynamics Numerics, Algorithms, Parallelization, Applications; M. Griebel, S. Knapek, G. Zumbusch

[17] Goran Wahnstrom MOLECULAR DYNAMICS 2013 Lecture notes

[18] The Art of Molecular Dynamics Simulation, D.C Rapaport

[19] The Mechanics and Statistics of Active Matter." S. Ramaswamy, Annu. Rev. Condens. Matter Phys. 1, 323 (2010).

[20] A Wall of Funnels Concentrates Swimming Bacteria." P. Galajda, J. Keymer, P. Chaikin, and R. Austin, J. Bacteriol. 189, 8704 (2007).

[21] Structure and Dynamics of a Phase-Separating Active Colloidal Fluid." G.S. Redner, M.F. Hagan, and A. Baskaran, Phys. Rev. Lett. 110, 055701 (2013).

[22] Anomalous structural and mechanical properties of solids confined in quasi one dimensional strips Debasish Chaudhuri, Surajit Sengupta

[23] $g(r) \to 1$ for $r \to \infty$, but in our plots it deviates slightly from 1 due to the fact that while counting particle pairs we have considered all the particles within the cluster. But in the normalization factor, i.e $1/2\pi\rho r dr$, the radius r can extend to the regions which lie outside the cluster. It makes the large r limit of $g(r)$ to get suppressed below 1. This has to be corrected.

Chapter 7

Supplimentary Materials

7.1 Software Tools

A major part of this work is based on molecular dynamics simulations which we wrote from scratch. So we should specify the software tools that we used for that.

1. `g++` from GNU Compiler Collection GCC 4.8, written in C++11 standard.

2. `python` with `numpy` & `matplotlib` for some earlier codes.

3. `MPICH`, an implementation of the Message Passing Interface MPI 2.2 for parallelization.

4. `Eigen`, a header-only linear algebra library for C++

5. Qt API's QImage class for generating configuration images.

6. `gnuplot` for general plotting

7. Eclipse & QtCreator IDE for managing long codes.

8. RStudio (a GUI for R programming language), for some analysis.

9. All of these work was done in a GNU/Linux environment, in Arch Linux, xubuntu & CentOS.

7.2 Codes

`https://github.com/sphCow/parallel-md`